Heliyon 6 (2020) e05292

Contents lists available at ScienceDirect

Heliyon

journal homepage: www.cell.com/heliyon

Research article

Enhanced electrochemical performance of flexible and eco-friendly starch/graphene oxide nanocomposite

Muhammad Rakibul Islam *, Shafiqul I. Mollik

Department of Physics, Bangladesh University of Engineering and Technology (BUET), Dhaka, Bangladesh

ARTICLE INFO

Keywords:
Materials science
Nanotechnology
Starch
Graphene oxide
Specific capacitance
Mechanical properties
Electrochemical properties

ABSTRACT

In this work, flexible plasticized starch/graphene oxide (PS/GO) nanocomposites are synthesized by a simple and economic solution cast technique. The structural and surface morphological study of the nanocomposite demonstrates an increased degree of interaction between PS and GO which in turn improves the mechanical strength and thermal stability of the nanocomposite. The influence of GO loading on the capacitive performance of the nanocomposite was evaluated by studying the electrochemical properties. The PS/GO nanocomposite showed an improved capacitive behavior with a specific capacitance of 115 F/g compared to that of pure starch (2.20 F/g) and GO (10.42 F/g) at a current density 0.1 mA/cm^2. The electrochemical impedance analysis indicates that the incorporation of GO enhances the conductivity of the nanocomposite in the charge transfer resistance at the electrode/electrolyte interface due to the incorporation of GO. The large surface areas provided by the GO sheets allow faster transport of charge carriers into the electrode and improve the electrochemical properties of the PS/GO nanocomposite. Considering the simplicity and effectiveness of the synthesis proses, the result indicates that the PS/GO nanocomposite could be a potential alternative for bio-friendly, flexible energy-storage applications.

1. Introduction

Recently, electrochemical energy storage has received significant research interest because of its high power density, extended lifecycle together with the friendliness to the environment of the supercapacitors compared to the secondary batteries and their wide range of applications in portable electronics to electric automotive [1, 2, 3]. To date, a variety of polymers based nanocomposite obtained from PVA, PEDOT, PANI, polyaniline, polypyrrole, etc. showed high-performance energy storage properties [2,3]. Most of these polymers originate from the synthetic route and are not readily degradable, which may cause a great threat to the environment. Therefore, considering its potential in energy storage applications, coupled with its enhanced economic viability and sustainability, biopolymer-based energy storage devices have garnered immense prominence when compared to the non-biodegradable polymer. Electrochemical devices fabricated from natural biocompatible materials are low cost as they are abundant in nature and environment friendly and have the ability to address the environmental hazard produced by non-degradable devices [4,5]. More specifically, biopolymers obtained from renewable sources are considered as the building block of environment-friendly energy storage devices. To date, a variety of biopolymers obtained from natural sources demonstrated diverse applications in different branches, such as electronics, display, energy storage, etc. [6, 7, 8, 9, 10]. In particular, Starch, a natural polysaccharide, is considered as one of the most promising natural biopolymers as it possesses a number of unique specialties such as renewability, abundance, low cost, and biodegradability [4,5].

Incorporation of nanofillers into the polymer matrix is a prevalent technique to enhance the thermal, electrical, and mechanical performance of the biopolymer. Allotropes of carbon such as carbon nanotubes, and graphene are being widely used as fillers for polymer matrix [11, 12, 13, 14, 15, 16]. Among them, graphene, a truly two-dimensional (2D) material, arranged in a hexagonal lattice, has considered as the most efficient nanofillers due to its unique chemical and physical properties. Graphene oxide (GO), a derivative of graphene, has attracted significant research attention as a nanofiller due to its distinctive advantages, including low cost, facile mass production, and extraordinary mechanical properties. Additionally, the abundant oxygen functional groups in GO allows the formation of hydrogen bond interactions with starch [17, 18, 19]. Besides, the higher stability of GO suspension in water allows

* Corresponding author.
E-mail address: rakibul@phy.buet.ac.bd (M.R. Islam).

https://doi.org/10.1016/j.heliyon.2020.e05292
Received 16 June 2020; Received in revised form 14 August 2020; Accepted 14 October 2020

preparation of starch/GO composites using solution-processed techniques which are simple and economic.

Graphene oxide reinforced starch nanocomposite has been synthesized and characterized by a number of research groups and GO was found to boost the mechanical performance and increase the thermal stability of the materials [20, 21, 22]. Li et. al. have synthesized PS/GO nanocomposite and demonstrate that the addition of GO into the matrix enhances the mechanical performance of the nanocomposite remarkably [20]. Zheng et. al. showed that incorporation of GO into the PS matrix enhances the absorbance in the UV region and may be used as a UV protector [21]. Bhattacharyya et. al. showed that PS/GO nanocomposite can remove organic dye from aqueous solution and can be used for the decontamination of water [23]. Aqda et. al. have shown that graphene oxide/starch nanocomposite can be used to extract antibiotics from milk [24]. Even though a countable work has been performed on GO-based starch nanocomposite, most of them focusing on the enhancement of optical, thermal, and mechanical performance of the nanocomposite however detailed investigation on the electrochemical performance of GO/starch was inadequate. Therefore, the main goal of this research is to investigate the influence of GO nanofiller on the electrochemical properties of PS/GO nanocomposite.

In this article, one of the promising applications of PS/GO nanocomposite, the energy storage capacity has been reported. The synthesis method is one of the major factors that control the surface morphology, structure, and electrochemical performance of the nanocomposite. We have chosen a solution cast technique for the synthesis of PS/GO nanocomposite since GO suspension was unwavering in water because of their plentiful oxygen-containing groups. Solution casting has several other advantages including easy and simple setup, low processing time, and cost-effectiveness. The influence of GO loading on the structural parameters, surface morphology, thermal stability, and mechanical properties of the nanocomposite was studied. To appraise the use of PS/GO nanocomposites for energy storage applications, the electrochemical properties of pure PS and PS/GO were studied in detail by cyclic voltammetry (CV), galvanostatic charge-discharge (GCD) measurement, and Electrochemical impedance spectroscopy (EIS) analysis. PS/GO nanocomposite exhibit improved electrochemical performance together with significantly enhanced specific capacitances, originating from the synergistic effect of PS and GO.

2. Materials and characterization

2.1. Materials

Graphite fine powder (Loba Chemie, India) company, Potassium permanganate ($KMnO_4$) (Merck, India), hydrogen peroxide (H_2O_2) (Qualikems, India), sodium nitrate ($NaNO_3$), sulfuric acid (H_2SO_4, 98%), were obtained from the supplier, all analytical grade or better and used as received. Starch was extracted in our laboratory from Potato.

2.2. Sample preparation

Modified Hummers method was used to prepare GO [25]. At first, 5 g natural graphite fine powder, 2.5 g $NaNO_3$, and 115 mL H_2SO_4 were poured into a glass pot followed by stirring in an ice-bath followed by mixing of 15 g $KMnO_4$ under continuous stirring and care was to kept the temperature less than 200 °C. The mixture was heated and stirred for a few hours followed by the addition of de-ionized water in an oil bath at 95 °C. After that aqueous solution of H_2O_2 was mixed to diminish the residual $KMnO_4$ until the bubble got disappeared. After filtering the solution the residue was washed by hot water until it becomes neutral.

Figure 1 (a) shows the X-ray diffraction (XRD) pattern of the GO flakes. The XRD spectra of GO gives a sharp (001) peak at 10.4°, suggesting an interlayer spacing of 8.0 $\dot{A}$ between the layer of GO. This increment suggests presence of oxygen congaing groups at the carbon basal plane of GO [26].

Figure 1 (b) shows the Fourier-transform infrared spectroscopy (FTIR) spectrum of GO. A wide band corresponds to OH groups is observed between 3550-3000 cm^{-1}. This suggests that inter- and intramolecular hydrogen bonding are present in the as-prepared GO. Peaks are also observed at 1066 cm^{-1} (C–O–C, C–O bond), and 1720 cm^{-1} (CO, C=O bond of carbonyl and carboxyl groups) [27]. These peak confirms existence oxygen groups at GO. The bands at 2926 cm^{-1}, 1625 cm^{-1}, and 1384 cm^{-1} indicates the stretching of C–H, C=C, and C–O bond respectively [28].

To synthesize starch, the clean potato was grated and put into a mortar followed by grinding in DI water. Then the liquid was poured off to a beaker. This process was repeated several times. The decantation of water leaves potato starch at the beaker. The starch was then dried for an hour. Since starch is made of long chains of glucose, vinegar was used to break down the chains. Propane-1, 2, 3-triol (glycerol) was added to plasticize the starch. To synthesize potato starch/graphene oxide (PS/GO) nanocomposite, at first, an aqueous solution of GO powder was made and the solution followed by an hour of sonication yielding uniformly dispersed GO solution. Two different concentration of GO fillers (0.5 wt% and 1.0 wt%) was used to prepare the PS/GO composite. To fabricate PS/GO composite, 5 g PS powder, 1.5 g glycerol, and 1.5 ml vinegar were mixed the GO solution. The blend was stirred constantly at 95 °C for 15 min for plasticization of starch. The PS/GO solution was then decanted onto a petri dish followed by heating at 50 °C yielding solid films. Three different nanocomposite films were made and named as PS, PS/GO (0.5%), and PS/GO (1%), where the number inside the parenthesis represented the loading of GO.

2.3. Characterization methods

The structural properties of the nanocomposites was investigated by an X-ray diffractometer (3040XPert PRO, Philips) using monochromatic CuK_α radiation ($\lambda = 1.54Å$). FTIR spectra of the nanocomposites were

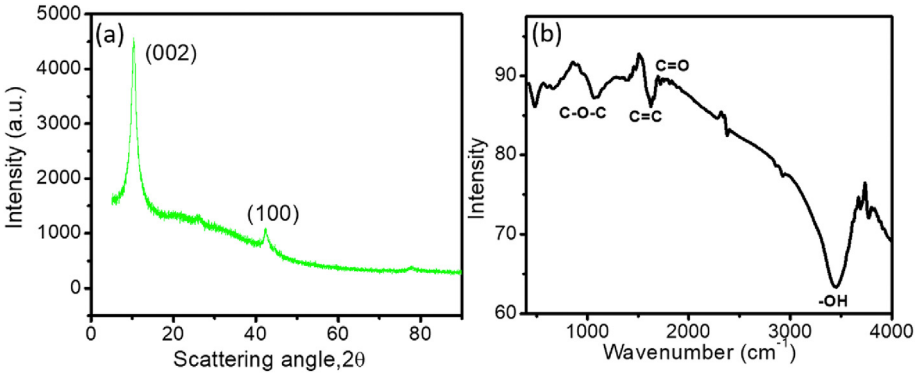

Figure 1. (a) XRD patterns and (b) FTIR spectrum of the GO powder.

studied using an FTIR spectrometer (IRSpirit, Shimadzu). The thermal properties of PS/GO nanocomposites were investigated by a thermogravimetric analyzer (TGA) (TG50, Shimadzu). The TGA curves were studied at the temperature ranges between 25 °C and 800 °C under a nitrogen atmosphere.

The tensile properties of the composites were studied using universal testing machine (Wance ETM 501) at ambient using a 10N load cell at a crosshead speed of 10 mm/min. The standard test method for tensile properties of thin plastic sheeting (specification D882-02) was followed. An average value of five replicates for each sample was taken for the tensile tests. After the tensile test, the fractured surface of the PS and PS/GO composite was observed by a field emission scanning electron microscope (FE-SEM) (JEOL-JSM 7600) at an accelerating voltage of 5 kV.

The electrochemical measurements were performed in 0.1M KCL solution using an electrochemical workstation (CorrTest CS310) at room temperature. The measurements were carried out by using a three-electrode cell configuration: Ag/AgCl reference electrode, polished Glassy Carbon with electro-active material (2 mg) as the working electrode, and platinum plate (1 cm × 1 cm) counter electrode.

3. Results and discussions

3.1. Structural properties of the nanocomposite

XRD was performed to investigate the crystalline structure of neat PS and PS/GO nanocomposite and the corresponding XRD pattern is shown in Figure 2. Generally, starch are classified into A, B, and C forms [29]. In Figure 2, the intense diffraction occurred at $2\theta = 17°$ together with several peaks near 20°, 22°, and 24°, indicating B-type crystal morphologies of the PS [30,31]. XRD patterns of PS/GO composites appearing almost the same peaks as PS signifies that PS/GO nanocomposite contains the same crystal type as PS. Additionally, the characteristic diffraction peak of GO was disappeared in the XRD pattern of PS/GO and the intensity of all the diffraction peak was decreased suggesting that the addition GO the deteriorate the crystallinity of the PS matrix. Furthermore, it is observed that the incorporation of GO (0.5%) upshift the peaks indicating a reduction in the *d*-spacing [32]. Whereas incorporation of 1.0% GO downshifted the peaks meaning an increase in the *d*-spacing.

3.2. Fourier transform infrared spectroscopy

FTIR spectroscopy was used to study the chemical changes that occur in PS after the addition of filler. The FTIR spectra of PS and PS/GO nanocomposites are presented in Figure 3. For PS film, the bands at 3352 cm^{-1} and 1651 cm^{-1} corresponds to the presence of –OH groups [33]. The band at 2941 cm^{-1} corresponds to the C–H stretching vibration of

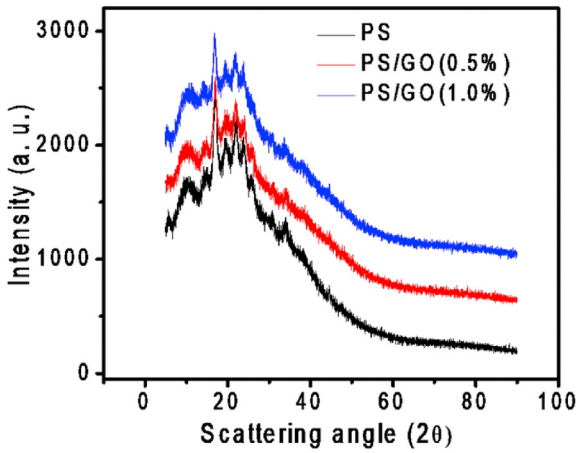

Figure 2. XRD patterns of PS and PS/GO nanocomposites.

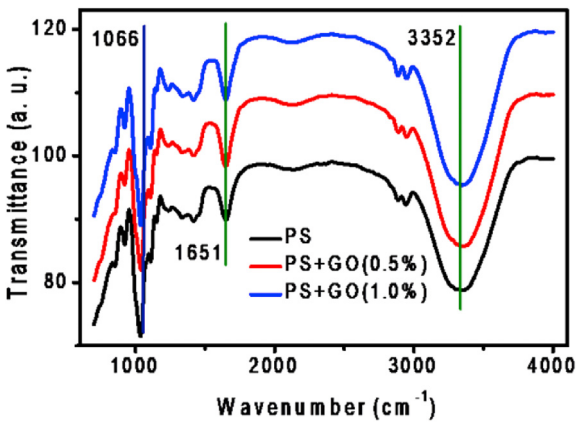

Figure 3. FTIR spectra of PS/GO nanocomposites with concentration of GO added to 0%, 0.5% and 1.0%.

methane hydrogen atoms [34]. The bands at 1151 cm^{-1} and 1109 cm^{-1} represents the presence of C–O bond in the anhydrous glucose ring. The PS/GO nanocomposite exhibit all of these major characteristics of the PS matrix. The OH banding has been shifted to the lower wavenumber in the PS/GO nanocomposite, suggesting that formation of hydrogen bonding between the polymer and filler [20]. Besides, the intensity of the band corresponds to the OH group (at 3352 cm^{-1}) increases with the incorporation of GO. This suggests that the incorporation of GO into the PS matrix enhances the hydrophilicity of the surface [35]. Overall, the FTIR spectra of PS/GO nanocomposite indicate the presence of strong interaction between GO with the PS matrix, and no new bond was formed between them [36].

3.3. Surface morphology

The morphology of the fractured surfaces of the PS/GO composites is presented in Figure 4. The granular structure of starch was absent in the morphology of the pure PS film. GO was found to be evenly distributed over the PS matrix. For the higher concentrations of GO, a few agglomerations were observed in the composite. The presence of plentiful oxygen-containing groups of GO allows formation of interaction between PS and GO by hydrogen bonding [37]. Furthermore, the GO surface observed to be enclosed by the polymer, suggesting presence of strong interfacial interactions between GO and PS.

3.4. Thermal stability of the nanocomposite

Thermal analysis of the nanocomposite was performed by thermogravimetric analysis (TGA) to analyze the influence of GO on the thermal decomposition behavior of PS. Figure 5 shows the TG curve of the PS and PS/GO nanocomposite. Two main thermal events are observed in the TG curve for PS. The first one, before the onset temperature (~100 °C), can be attributed to the volatilization of the water absorbed by starch and glycerol plasticizer [38]. The second event occurred between 220 °C to 380 °C corresponded to the elimination of polyhydroxyl group and starch decomposition [39]. The TG curve for PS/GO nanocomposite represents similar behavior except for the residual mass at 800 °C, which can be attributed to the presence of more stable GO in the PS matrix.

The different thermal parameters, such as the initial decomposed temperature (IDT), integral procedural decomposition temperature (IPDT), the temperature at 50% weight loss (T−50%), and the temperature at the maximum rate of mass loss (T_{max}) were calculated [40] from the TG curve of the nanocomposite to assess the thermal stability of the material's and are presented in Table 1. It could be observed that all the PS/GO possesses a higher IPDT than neat PS, signifies the increases of the decomposition temperatures of PS due to the incorporation of GO. This may be due to the suppression of the mobility of PS by strong hydrogen

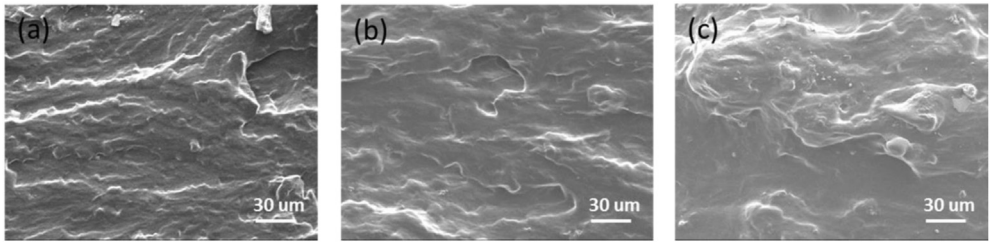

Figure 4. FESEM images of the cross-sections of PS/GO nanocomposites with concentration of GO added to (a) 0%, (b) 0.5% and (c) 1.0%.

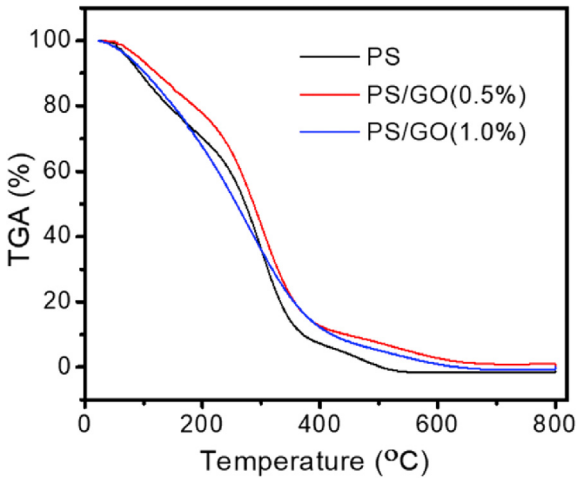

Figure 5. TGA thermograms of PS and PS/GO nanocomposites film with concentration of GO added to 0%, 0.5% and 1.0%.

interactions of GO. Typically, the better interaction between nanofiller and polymer resulting in improved thermal stability of the nanocomposites [41]. Though, PS/GO (1.0%) nanocomposites thermally degraded at a temperature lower than that of PS/GO (0.5%) suggesting that addition of more GO reduces the thermal stability of the PS/GO composites. With the increase of GO content, the decomposition of oxygen functional groups weakens the interaction between polymer matrix and nanofiller resulting in faster decomposition of the starch matrix [42].

3.5. Mechanical properties

The effects of the concentration of GO nanofiller on the mechanical performance of PS/GO nanocomposite are illustrated in Figure 6. Figure 6(a) shows the influence of GO nanofiller on the tensile properties of PS/GO nanocomposites. The tensile strength of pure PS was 20 MPa. The tensile strength reached 42 MPa for 1 wt% GO loading. Besides, the elongation at break of the nanocomposites also increases as the concentration of GO increases. The elongation at break shows an opposite trend and it decreased from 67% to 45% when 0.5% GO was added to the PS matrix. An increase in GO loading to 1.0% increases the elongation at break to 70%. Figure 6(b) demonstrates the variation of Young modulus of the PS/GO nanocomposites as a function of GO loading. A 16% increase in the tensile modulus from 40.8 MPa to 47.3MPa has been observed when 0.5wt % GO is added to the matrix. A further increase in GO (1wt %) concentration resulting in a 40% rise of the tensile modulus.

From Figure 6 it is observed that the incorporation of GO enhanced the tensile performance of the composite signifies that GO has a reinforcing effect on the PS matrix. Usually, the improvement of mechanical properties of polymer nanocomposite depends on i) interfacial interaction among the nanofillers and matrix and ii) good dispersion of nanofiller [43]. The observed enhancement in the mechanical performance of the nanocomposite suggests well-dispersion [37] of the GO nanofiller into the PS matrix. Hydrogen-bonding interactions created between the oxygen-containing groups of GO and the OH groups of starch which leads to good interfacial interaction among them [20]. As a consequence, it is very difficult to disconnect the GO nano-filler from the matrix and they weaken the tensile stress by transferring them to the PS/GO interfaces, resulting in improved tensile properties.

3.6. Electrochemical properties of the nanocomposite

Cyclic voltammograms (CV) measurements were performed to study how the GO nanofiller influence the capacitive performance of the nanocomposite. CV data were taken at different sweep rates (5 mVs^{-1}, 10 mVs^{-1}, 20 mVs^{-1}, 30 mVs^{-1}, 50 mVs^{-1} and 80 mVs^{-1}) in a potential window of 10 V (Figure 7). In all cases, the area of the CV loop increases with the sweep rate. For all scan rates, the CV curves for PS exhibit nearly rectangle cyclic voltammograms whereas a distorted rectangular shape is observed for the GO and PS/GO composite. Such deviation can be attributed to the presence of pseudocapacitance resulting from the oxygen groups on the GO surface and the presence of uncompensated resistance due to the GO flake in the system [44]. Additionally, the CV for GO and PS/GO composite exhibits a sharp rise in current at a low voltage which drops sharply at the vertex potential suggesting that incorporation of GO improves the capacitive performance of the nanocomposite [45].

Figure 8 (a) shows the CV measurements for PS, GO, PS/GO (0.5%) and PS/GO (1.0%) at 20 mVs^{-1}. Notably, the quasi-rectangle area of CV graphs of PS/GO was larger than that of pure PS and pure GO, indicating the better capacitive performance of PS/GO composites. This indicates that the GO nanofiller speeds up the carriers' transportation along with the PS matrix [46]. Figure 8(b) represents the galvanostatic charge-discharge (GCD) graphs of PS and PS/GO nanocomposite at a constant current density of 0.1 mA/cm^2. The discharging curve PS/GO (0.5%) showed two voltage ranges. A short discharge occurred between 0.8 V to 0.4V due to the electric double-layer capacitance (EDLC) formed due to the charge separation between the electrode and electrolyte interface. A longer discharge occurred between 0.4V to -0.2V which may be attributed to the combination of EDLC and Faradaic capacitance [47]. The IR drop during discharging of the GCD curve gives an idea about the

Table 1. Thermal parameters of PS and PS/GO nanocomposite obtained from TGA curves.

Sample	IDT (C)	IPDT (C)	T-50% (C)	T_{max} (C)
PS	242	243	273	380
PS/GO (0.5%)	253	284	286	380
PS/GO (1%)	225	264	258	346

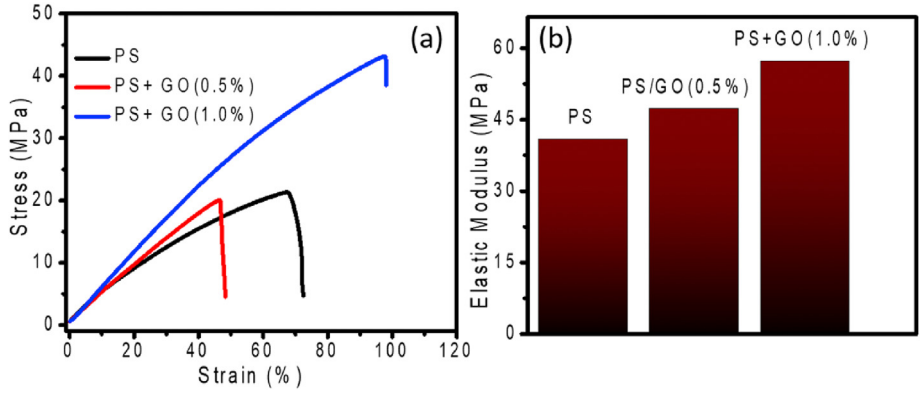

Figure 6. Effect of GO concentrations on (a) tensile properties and (b) Young's modulus of PS/GO nanocomposites.

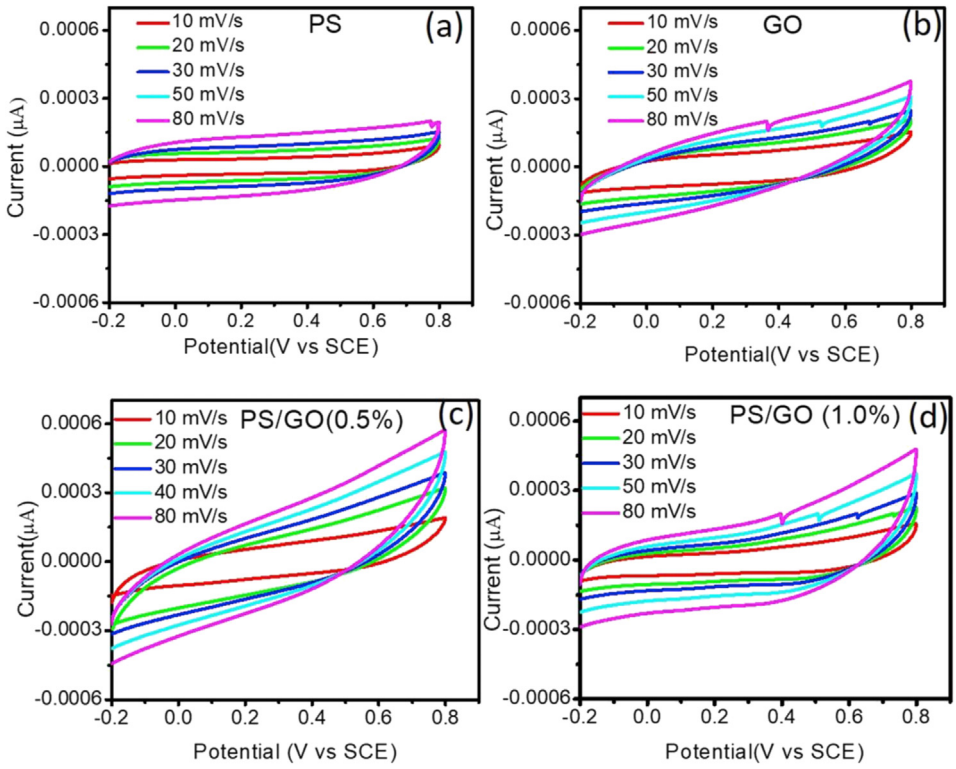

Figure 7. Cyclic Voltammetry curves of (a) PS, (b) GO, (c) PS/GO (0.5%), and (d) PS/GO (1.0%) electrodes at different scan rate with current density of 0.1 mA/cm.^{2}.

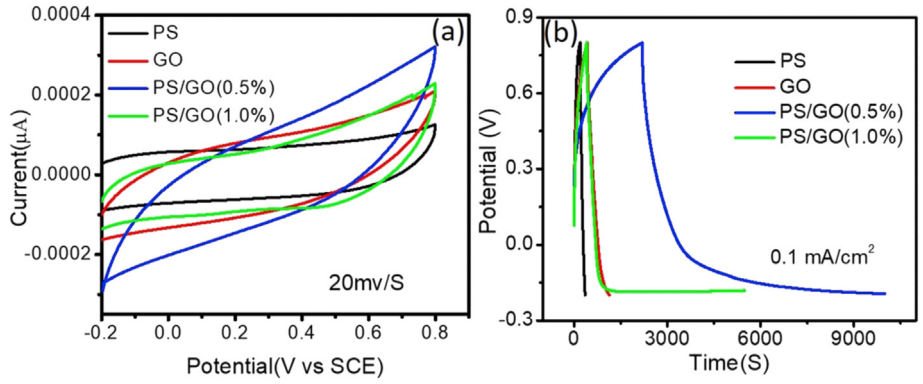

Figure 8. (a) CV graphs of PS, GO, and PS/GO electrodes at sweep rates 20 mV/S and (b) GCD graphs of PS, GO, PS/GO electrodes.

Table 2. Electrochemical parameters of PS, GO, PS/GO (0.5%) and PS/GO (1.0%) at 0.1 mA/cm^2

Samples	Specific Capacitance (F/g)	Energy Density (Wh/kg)	Power Density (W/kg)	Cyclic Stability (%)	Rate Capability (%)
PS	2.20 ± 0.32	0.33	7.41		58.33
GO	10.45 ± 0.62	1.50	7.47		41.55
PS/GO (0.5%)	115.00 ± 1.70	16.14	7.55	86.88%	38.17
PS/GO (1.0%)	75.10 ± 1.20	10.59	7.53	85.80%	34.79

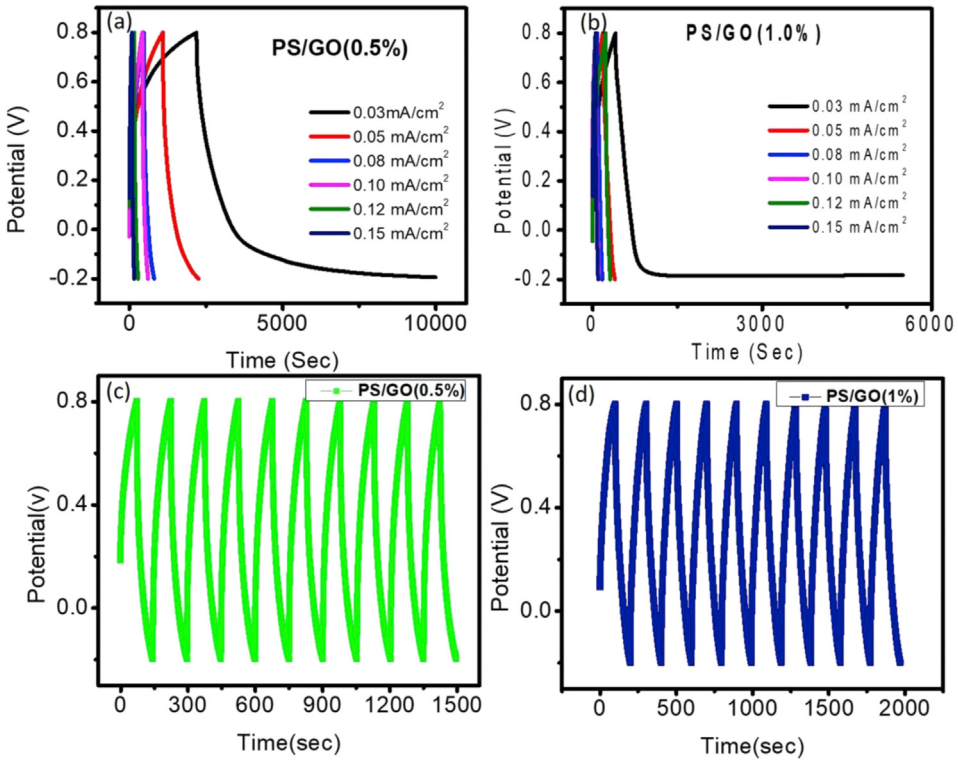

Figure 9. GCD curves for (a) PS/GO (0.5%) and (b) PS/GO (1.0%) composite at different current densities. GCD curves for ten cycle at 0.1 mA/cm^2 for (c) PS/GO (0.5%) and (d) PS/GO (1.0%) nanocomposite.

internal resistance of the electrode [48]. The IR drop of PS/GO (0.5%) was found to be the smallest of all the different nanocomposites suggesting the presence of low internal resistances of the PS/GO (0.5%) nanocomposite. For materials with low internal resistance, energy dissipation during charging-discharging processes got diminished and thereby improve the energy storage performance. Thus, PS/GO (0.5%) nanocomposite is more suitable for fabricating power-saving supercapacitors.

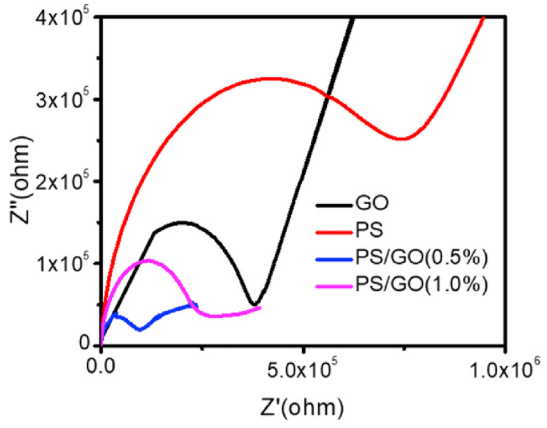

Figure 10. Nyquist plots of pure PS, GO and PS/GO electrodes at room temperature.

The specific capacitances (C_s) of the different nanocomposites were estimated from their respective GCD curve using the formula $C_s = I\Delta t/m\Delta V$ [49] where, I is the constant current (A), Δt is the discharge time (sec), ΔV is the potential window (V) and m is the mass of the active materials (g). The first discharge specific capacitances of PS, GO, PS/GO (0.5%), PS/GO (1.0%) composite electrodes were found to be 2.4F/g, 10.83F/g, 116.25F/g, and 76.15F/g, respectively. The average value of the specific capacitance, energy density, and power density of these composites are summarized in Table 2. It was evident that the specific capacitance for PS/GO was significantly larger than that of PS or GO. Figure 9 represents the GCD curves for the PS/GO (0.5%), PS/GO (1.0%) at different current density. Based on this data the rate capability of these electrodes was measured and was found to be 38% and 35% respectively. Furthermore for the PS/GO (0.5%) and PS/GO (1.0%) the GCD data were taken at 0.1 mA/cm^2 for a number cycle (figure 9 (c), (d)) from which the cyclic stability of the electrodes was calculated and are presented in Table 2.

From Table 2 it can be concluded that the significantly enhanced specific capacitances of PS/GO nanocomposite originates from the synergistic effect of PS and GO. Such an enhancement in the capacitance can be attributed to a number of factors. GO with higher specific surface area

increases the functioning area of the nanocomposite/electrolyte interface whereas the layered structure of GO diminishes the diffusion length of the electrolyte ions [50,51]. This improves the specific capacitance by increasing the electroactive region. Additionally, due to the hydrophilicity of GO, the ions can easily move to the electrode/electrolyte interface for PS/GO nanocomposite resulting in increased action site and high specific capacitance. However, agglomeration in of GO sheets may occur when the GO contents are increased, this can reduce the accessible surface area accessible for ion exchange leading to a decreased specific capacitance [52]. Besides, the XRD results suggest that the interlayer spacing increases with the increase of GO content, causing a decrement of the specific capacitance for higher GO content.

Electrochemical impedance spectroscopy (EIS) is a reliable technique to analyze the performance of electrochemical system, was performed to understand the kinetic aspect of the ion diffusion liable for the energy storage property of the electrode. The Nyquist plot of the composites electrodes is demonstrated in Figure 10, which allows the EIS investigation of the electrodes consisting of pure PS, GO, and PS/GO composites as a function of the frequency of the alternating current. Two semicircles are observed in the Nyquist plot. The semicircle at low frequency represents the grain boundary resistance and the other semicircle represents the resistance of grain or bulk [53]. Semicircular arc diameter is an important parameter for measuring the charge transfer resistance of the electrodes. In figure smaller semicircle at lower frequency indicates a lower faradic charge-transfer barrier at the grain boundary. Polar functional groups and corresponding defects are always present in GO and the disordered graphene lattice is responsible for the smaller Nyquist semicircle [54,55]. For PS/GO (0.5%), the radius of the semicircle at low-frequency regions is smallest suggesting that the height of the faradic charge-transfer barrier for the nanocomposite [56]. This also suggests that the incorporation of GO reduces the resistivity of the nanocomposite and thereby upsurges the charge transport properties of the nanocomposite. Additionally, the slope of the PS/GO composite was nearer to 90°, representing good capacitive quality [56]. In total, the electrochemical performance of the PS/GO nanocomposite obtained from the EIS analysis matches the results obtained from the CV and the GCD analysis.

4. Conclusions

In conclusion, Bio-friendly, PS/GO composites were synthesized using a simple solution casting process. Structural analysis of the nanocomposite demonstrates the presence of strong hydrogen bonding interaction between PS and GO, which results in improved mechanical and thermal properties of the nanocomposites. The electrochemical analysis demonstrates that the incorporation of GO improves the capacitive performance of the PS/GO nanocomposite and large specific capacitance (115 F/g) was observed for the PS/GO nanocomposite. EIS analysis reveals a reduction in charge transfer resistance at the electrode/electrolyte interface due to the incorporation of GO. The large specific capacitance of PS/GO nanocomposite can be attributed to the large surface areas provided by the GO sheets together with the increase of action ion resulting from the improved hydrophilicity caused by the GO nanofiller. Finally, it can be concluded that the PS/GO nanocomposite synthesized by an effective and economic method may open up a bio-friendly route that can be used in energy storage applications.

Declarations

Author contribution statement

Muhammad R. Islam: Conceived and designed the experiments; Analyzed and interpreted the data; Contributed reagents, materials, analysis tools or data; Wrote the paper.

Shafiqul I. Mollik: Performed the experiments; Analyzed and interpreted the data; Wrote the paper.

Funding statement

This work was supported by the Ministry of Science and Technology, Government of Bangladesh (39.00.0000.009.06.024.19/Phy's-532) and Bangladesh University Grants Commission (6 (74)/BMK/RSP/BOP/VOUT-(8)/2018/2601).

Competing interest statement

The authors declare no conflict of interest.

Additional information

No additional information is available for this paper.

References

[1] L.L. Zhang, X.S. Zhao, Carbon-based materials as supercapacitor electrodes, Chem. Soc. Rev. 38 (2009) 2520–2531.
[2] Q. Meng, K. Cai, Y. Chen, L. Chen, Research progress on conducting polymer based supercapacitor electrode materials, Nano Energy 36 (2017) 268–285.
[3] G.A. Snook, P. Kao, A.S. Best, Conducting-polymer-based supercapacitor devices and electrodes, J. Power Sources 196 (2011) 1–12.
[4] M.I. Vladu, E.D. Głowacki, P.A. Troshin, G. Schwabegger, L. Leonat, D.K. Susarova, Indigo – from jeans to semiconductors: indigo – a natural pigment for high performance ambipolar organic field effect transistors and circuits, Adv. Mater. 24 (2012) 375–380.
[5] M. Oliviero, R. Rizvi, L. Verdolotti, S. Iannace, H.E. Naguib, E. Di Maio, Dielectric properties of sustainable nanocomposites based on zein protein and lignin for biodegradable insulators, Adv. Funct. Mater. 27 (2017), 1605142.
[6] T. Lei, M. Guan, J. Liu, H.C. Lin, R.P. fattner, L. Shaw, A.F. McGuirec, et al., Biocompatible and totally disintegrable semiconducting polymer for ultrathin and ultralightweight transient electronics, Proc. Natl. Acad. Sci. 114 (20) (2017) 5107–5112.
[7] M.I. Vladu, P.A. Troshin, M. Reisinger, L. Shmygleva, Y. Kanbur, G. Schwabegger, et al., Biocompatible and biodegradable materials for organic field-effect transistors, Adv. Funct. Mater. 20 (23) (2010) 4069–4076.
[8] J. Xu, X. Zhao, Z. Wang, H. Xu, J. Hu, J. Ma, Y. Liu, Biodegradable natural pectin-based flexible multilevel resistive switching memory for transient electronics, Small 15 (4) (2018), 1803970.
[9] A. Sorrentino, G. Landi, S. Iannace, H.C. Neitzert, Differences between graphene and graphene oxide in gelatin based systems for transient biodegradable energy storage applications, Nanotechnology 28 (2017), 054005.
[10] M. Oliviero, R. Rizvi, L. Verdolotti, S. Iannace, H.E. Naguib, E. Di Maio, H.C. Neitzert, G. Landi, Bio-nanocomposites: dielectric properties of sustainable nanocomposites based on zein protein and lignin for biodegradable insulators, Adv. Funct. Mater. 27 (8) (2017), 1605142.
[11] L.M. Famá, V. Pettarin, S.N. Goyanes, C.R. Bernal, Starch/multi-walled carbon nanotubes composites with improved mechanical properties, Carbohydr. Polym. 83 (3) (2011) 1226–1231.
[12] D. Liu, P.R. Chang, et al., Fabrication and characterization of zirconium hydroxide-carboxymethyl cellulose sodium/plasticized Trichosanthes Kirilowii starch nanocomposites, Carbohydr. Polym. 86 (4) (2011) 1699–1704.
[13] Z. Liu, L. Zhao, M. Chen, J. Yu, Effect of carboxylate multi-walled carbon nanotubes on the performance of thermoplastic starch nanocomposites, Carbohydr. Polym. 83 (2) (2011) 447–451.
[14] P. Dallas, V.K. Sharma, R. Zboril, Silver polymeric nanocomposites as advanced antimicrobial agents: classification, synthetic paths, applications, and perspectives, Adv. Colloid Interface Sci. 166 (1–2) (2011) 119–135.
[15] S. Kumar, S. Raj, S. Jain, K. Chatterjee, Multifunctional biodegradable polymer nanocomposite incorporating graphene-silver hybrid for biomedical applications, Mater. Des. 108 (2016) 319–332.
[16] M. Zhang, Y. Li, Z. Su, G. Wei, Recent advances in the synthesis and applications of graphene–polymer nanocomposites, Polym. Chem. 6 (34) (2015) 6107–6124.
[17] Y. Feng, X. Zhang, Y. Shen, K. Yoshino, W.A. Feng, A mechanically strong, flexible and conductive film based on bacterial cellulose/graphene nanocomposite, Carbohydr. Polym. 87 (1) (2012) 644–649.
[18] J.R. Potts, D.R. Dreyer, C.W. Bielawski, R.S. Ruoff, Graphene-based polymer nanocomposites, Polymers 52 (1) (2011) 5–25.
[19] D. Cai, M. Song, Recent advance in functionalized graphene/polymer nanocomposites, J. Mater. Chem. 20 (37) (2010) 7906–7915.
[20] R. Li, C. Liu, J. Ma, Studies on the properties of graphene oxide-reinforced starch biocomposites, Carbohydr. Polym. 84 (1) (2011) 631–637.
[21] P. Zheng, T. Ma, X. Ma, Fabrication and Properties of Starch-Grafted Graphene Nanosheet/Plasticized-Starch Composites, Ind. Eng. Chem. Res. 52 (39) (2013) 14201–14207.
[22] D. Wu, H. Xu, M. Hakkarainen, From starch to polylactide and nano-graphene oxide: fully starch derived high performance composites, RSC Adv. 6 (59) (2016) 54336–54345.

[23] A. Bhattacharyya, B. Banerjee, S. Ghorai, D. Rana, I. Roy, G. Sarkar, et al., reusable graphene oxide-potato starch based cross-linked bio-composite adsorbent for removal of methylene blue dye, Int. J. Biol. Macromol. 116 (2018) 1037–1048.
[24] T.G. Aqda, S. Behkami, M. Raoofi, H. Bagheri, Graphene oxide-starch-based micro-solid phase extraction of antibiotic residues from milk samples, J. Chromatogr. A 1591 (2019) 7–14.
[25] W.S. Hummers, R.E. Offeman, Preparation of Graphitic Oxide, J. Am. Chem. Soc. 80 (1958), 1339.
[26] Z. Gao, J. Wang, Z. Li, W. Yang, B. Wang, M. Hou, et al., Graphene Nanosheet/Ni^{2+}/Al^{3+} Layered Double-Hydroxide Composite as a Novel Electrode for a Supercapacitor, Chem. Mater. 23 (15) (2011) 3509–3516.
[27] S. Stankovich, D.A. Dikin, R.D. Piner, K.A. Kohlhaas, A. Kleinhammes, Y. Jia, et al., Synthesis of graphene-based nanosheets via chemical reduction of exfoliated graphite oxide, Carbon 45 (7) (2007) 1558–1595.
[28] C. Gao, X. Yu, R.X. Xu, J.H. Liu, X.J. Huang, AlOOH-reduced graphene oxide nanocomposites: one-pot hydrothermal synthesis and their enhanced electrochemical activity for heavy metal ions, ACS Appl. Mater. Interfaces 4 (9) (2012) 4672–4682.
[29] H.F. Zobel, Starch crystal transformations and their industrial importance, Starch 40 (1) (1988) 1–7.
[30] F. Elsenhaber, W. Schulz, Monte carlo simulation of the hydration shell of double-helical amylose: A left-handed antiparallel double helix fits best into liquid water structure, Biopolymers 32 (12) (1992) 1643–1664.
[31] W. Shujun, Y. Jinglin, G. Wenyuan, Use of X-Ray Diffractometry (XRD) in the identification of Fritillaria according to geographical origin, Am. J. Biochem. Biotechnol. 1 (4) (2005) 199–203.
[32] J. Yu, J. Yang, B. Liu, X. Ma, Preparation and characterization of glycerol plasticized-pea starch/ZnO–carboxymethylcellulose sodium nanocomposites, Bioresour. Technol. 100 (11) (2009) 2832–2841.
[33] P.P. Peregrinoa, M.J.A. Sales, M.F.P. da Silva, M.A.G. Sole, L.F.L. da Silva, S.G.C. Moreira, et al., Thermal and electrical properties of starch–graphene oxide nanocomposites improved by photochemical treatment, Carbohydr. Polym. 106 (2014) 305–311.
[34] X. Ge, H. Li, L. Wu, P. Li, X. Mu, Y. Jian, Improved mechanical and barrier properties of starch film with reduced graphene oxide modified by SDBS, J. Appl. Polym. Sci. 134 (22) (2017), 44910.
[35] Y. Feng, N. Feng, G. Du, A green reduction of graphene oxide via starch-based materials, RSC Adv. 3 (44) (2013) 21466–21474.
[36] C. Wan, B. Chen, Reinforcement and interphase of polymer/graphene oxide nanocomposites, J. Mater. Chem. 22 (2010) 3637–3646.
[37] T. Ma, P.R. Chang, P. Zheng, X. Ma, The composites based on plasticized starch and graphene oxide/reduced graphene oxide, Carbohydr. Polym. 94 (1) (2013) 63–70.
[38] D. Schlemmer, R.S. Angelica, M.J.A. Sales, Morphological and thermomechanical characterization of thermoplastic starch/montmorillonite nanocomposites, Compos. Struct. 92 (9) (2010) 2066–2070.
[39] X. Ma, P.R. Chang, J. Yu, M. Stumborg, Properties of biodegradable citric acid-modified granular starch/thermoplastic pea starch composites, Carbohydr. Polym. 75 (1) (2009) 1–8.
[40] S-J. Park, H-C. Kim, Thermal stability and toughening of epoxy resin with polysulfone resin, J. Polym. Sci., Polym. Phys. Ed. 39 (2001) 121–128.
[41] V. Mittal, Functional polymer nanocomposites with graphene: a review, Macromol. Mater. Eng. 299 (8) (2014) 906–931.
[42] S.L. Qiu, C.S. Wang, Y.T. Wang, C.G. Liu, X.Y. Chen, H.F. Xie, et al., Effects of graphene oxides on the cure behaviors of a tetrafunctional epoxy resin, Express Polym. Lett. 5 (9) (2011) 809–818.
[43] E. Franco-Marquès, J.A. Méndez, M.A. Pèlach, F. Vilaseca, J. Bayer, P. Mutjé, Influence of coupling agents in the preparation of polypropylene composites reinforced with recycled fibers, Chem. Eng. J. 166 (3) (2011) 1170–1178.
[44] J. Zhang, X.S. Zhao, Conducting polymers directly coated on reduced graphene oxide sheets as high-performance supercapacitor electrodes, J. Phys. Chem. C 116 (9) (2012) 5420–5426.
[45] Q. Wu, Y. Xu, Z. Yao, A. Liu, G. Shi, Supercapacitors based on flexible graphene/polyaniline nanofiber composite films, ACS Nano 4 (4) (2010) 1963–1970.
[46] K.A. Janani, K. Karunarathne, K.S. Perera, K.P. Vidanapathirana, J.C. Pitawela, Fabrication and evaluation of an electrochemical double-layer capacitor with natural graphite electrodes and magnesium trifluoromethanesulfonate–based gel polymer electrolyte, J. Solid State Electrochem. 23 (2019) 2165–2171.
[47] D. Wang, F. Li, J. Zhao, W. Ren, Z. Chen, J. Tan, et al., Fabrication of graphene/polyaniline composite paper *via In Situ* Anodic electropolymerization for high-performance flexible electrode, ACS Nano 3 (7) (2009) 1745–1752.
[48] Y. Xie, H. Du, Electrochemical capacitance of a carbon quantum dots–polypyrrole/titania nanotube hybrid, RSC Adv. 5 (2015) 89689–89697.
[49] S.J. Bao, C.M. Li, C.X. Guo, Y. Qiao, Biomolecule-assisted synthesis of cobalt sulfide nanowires for application in supercapacitors, J. Power Sources 180 (1) (2008) 676–681.
[50] N.G. Prakash, M. Dhananjaya, A.L. i Narayana, H. Maseed, V.V.S.S. Srikanth, O.M. Hussain, Improved electrochemical performance of rGO-wrapped MoO_3 nanocomposite for supercapacitors, Appl. Phys. A 125 (2019), 488.
[51] C. Xiong, B. Li, X. Lin, H. Liu, Y. Xu, J. Mao, C. Duan, T. Li, Y. Ni, The recent progress on three-dimensional porous graphene-based hybrid structure for supercapacitor, Compos. B Eng. 165 (2019) 10–46.
[52] A.G. Pandolfo, A.F. Hollenkamp, Carbon properties and their role in supercapacitors, J. Power Sources 157 (2006) 11–27.
[53] R.C. Kambale, P.A. Shaikh, C.H. Bhosale, K.Y. Rajpure, Y D Kolekar, Dielectric properties and complex impedance spectroscopy studies of mixed Ni–Co ferrites, Smart Mater. Struct. 18 (2009), 085014.
[54] K.A. Mkhoyan, A.W. Contryman, J. Silcox, D.A. Stewart, G. Eda, C. Mattevi, et al., Atomic and electronic structure of graphene-oxide, Nano Lett. 9 (3) (2009) 1058–1063.
[55] C. Gomez-Navarro, J.C. Meyer, R.S. Sundaram, A. Chuvilin, S. Kurasch, M. Burghard, et al., Atomic structure of reduced graphene oxide, Nano Lett. 10 (4) (2010) 1144–1148.
[56] W. Wu, Y. Li, L. Yang, Y. Ma, D. Pan, Y. Li, A facile one-pot preparation of dialdehyde starch reduced graphene oxide/polyaniline composite for supercapacitors, Electrochim. Acta 139 (2014) 117–126.